European Journal of Pharmaceutics and Biopharmaceutics 140 (2019) 109–120

Contents lists available at ScienceDirect

European Journal of Pharmaceutics and Biopharmaceutics

journal homepage: www.elsevier.com/locate/ejpb

Research paper

Selection of the optimal macrocyclic chelators for labeling with ^{111}In and ^{68}Ga improves contrast of HER2 imaging using engineered scaffold protein ADAPT6

Emma von Witting[a,1], Javad Garousi[b,1], Sarah Lindbo[a], Anzhelika Vorobyeva[b], Mohamed Altai[b], Maryam Oroujeni[b], Bogdan Mitran[c], Anna Orlova[c], Sophia Hober[a,*], Vladimir Tolmachev[b]

[a] Department of Protein Science, KTH – Royal Institute of Technology, SE-10691 Stockholm, Sweden
[b] Department of Immunology, Genetics and Pathology, Uppsala University, SE-75185 Uppsala, Sweden
[c] Department of Medicinal Chemistry, Uppsala University, Uppsala, Sweden

ARTICLE INFO

Keywords:
ADAPT
HER2
Radionuclide imaging
Indium-111
Gallium-68
DOTA
NOTA
NODAGA
DOTAGA

ABSTRACT

Radionuclide molecular imaging is a promising tool that becomes increasingly important as targeted cancer therapies are developed. To ensure an effective treatment, a molecular stratification of the cancer is a necessity. To accomplish this, visualization of cancer associated molecular abnormalities *in vivo* by molecular imaging is the method of choice. ADAPTs, a novel type of small protein scaffold, have been utilized to select and develop high affinity binders to different proteinaceous targets. One of these binders, ADAPT6 selectively interacts with human epidermal growth factor 2 (HER2) with low nanomolar affinity and can therefore be used for its *in vivo* visualization. Molecular design and optimization of labeled anti-HER2 ADAPT has been explored in several earlier studies, showing that small changes in the scaffold affect the biodistribution of the domain. In this study, we evaluate how the biodistribution properties of ADAPT6 is affected by the commonly used maleimido derivatives of the macrocyclic chelators NOTA, NODAGA, DOTA and DOTAGA with the aim to select the best variants for SPECT and PET imaging. The different conjugates were labeled with ^{111}In for SPECT and ^{68}Ga for PET. The acquired data show that the combination of a radionuclide and a chelator for its conjugation has a strong influence on the uptake of ADAPT6 in normal tissues and thereby gives a significant variation in tumor-to-organ ratios. Hence, it was concluded that the best variant for SPECT imaging is ^{111}In-(HE)$_3$DANS-ADAPT6-GSSC-DOTA while the best variant for PET imaging is ^{68}Ga-(HE)$_3$DANS-ADAPT6-GSSC-NODAGA.

1. Introduction

The major advantage of targeted anti-cancer therapeutics, such as monoclonal antibodies and their derivatives, is their selectivity. Molecular recognition of tumor-specific antigens focuses the action on malignant cells and enables a substantial reduction of toxicity to healthy tissues. Human epidermal growth factor receptor type 2 (HER2) is a molecular target for the humanized monoclonal antibodies trastuzumab (Herceptin), pertuzumab (Perjeta) and the antibody-drug conjugate trastuzumab-DM1 (Kadcyla). Treatment using these antibodies significantly improves survival of patients with HER2-positive breast cancer [1,2]. Still, only patients with HER2 overexpression can benefit from such treatment thus sufficiently high level of expression of the therapeutic target is a precondition for successful treatment [3]. The use of radionuclide molecular imaging of HER2 in disseminated cancer is a non-invasive approach potentially permitting visualization of molecular target expression in all metastases [4]. For nearly 20 years, development of sensitive and specific probes for imaging of HER2 remains one of the important issues to be solved by nuclear medicine [5,6]. The radiolabeling of therapeutic monoclonal antibodies is a facile way for generation of molecular imaging probes. However, there are two major issues in the use of monoclonal antibodies; slow clearance from blood necessitating several days delay between injection and imaging, and unspecific accumulation in target-negative tumors. Both issues are related to the large size of antibodies. It has been demonstrated earlier that the size reduction of targeting proteins, e.g. the use of antibody fragments improved both sensitivity and specificity of radionuclide imaging [5]. Single domain antibodies, sdAb, with the

* Corresponding author at: Department of Protein Science, CBH, KTH Royal Institute of Technology, Stockholm, Sweden.
E-mail address: sophia@kth.se (S. Hober).
[1] Contributed equally.

https://doi.org/10.1016/j.ejpb.2019.05.008
Received 11 February 2019; Received in revised form 7 May 2019; Accepted 9 May 2019
Available online 10 May 2019

molecular weight of approximately 15 kDa are currently the smallest immunoglobulin-based imaging probes, which provide very good imaging contrast at the day of injection [7].

An alternative approach for generation of small proteinaceous imaging probes is the use of engineered scaffold proteins (ESP), such as affibody molecules, adnectins, DARPins and ADAPTs [7]. A scaffold part of ESP provides a rigid support for variable amino acids minimizing the entropic penalty for binders selected using combinatorial libraries. This enables selection of binders with very high affinity (up to picomolar values) to desirable molecular targets. The molecular weight of ESP is typically in the range of 4–15 kDa, which is associated with a small size providing rapid extravasation into tumors. The small size ensures also a rapid clearance of the probes from circulation, which is required for a high contrast and, therefore, sensitivity of imaging. Radiolabeled ESP have demonstrated exceptional imaging contrast at the day of injection both in preclinical and clinical studies [7]. However, only a limited number of ESP have been evaluated for radionuclide imaging applications. Optimization of imaging properties of different ESP is a precondition for their successful application for radionuclide diagnostics.

By utilizing the three-helix scaffold of the albumin binding domain (ABD) of streptococcal protein G, a new type of engineered affinity proteins has been developed [8]. This scaffold protein has been denoted ADAPT (ABD-Derived Affinity ProTein). The ADAPT scaffold contains 46–61 amino acids, i.e. it is sufficiently small for imaging applications. Selections from the library, which was created by randomization of eleven amino acids, provided ADAPTs binding specifically to human epidermal growth factor receptor 3 (HER3) [9], tumor necrosis factor-α (TNF-α) [10], and HER2 [11]. For the HER2-binding ADAPT, several variants with different affinities to albumin were selected [11]. To enable rapid blood clearance for use as a radionuclide imaging probe, an ADAPT variant, denoted ADAPT6, which does not bind to albumin, was developed [12]. A proof-of-principle study confirmed the feasibility of specific *in vivo* imaging of HER2 using ADAPT6 labelled with ^{111}In and ^{68}Ga [12]. Several further studies enabled the refinement of the molecular design of ADAPT6-based probes for imaging of HER2. Particularly, the influence of the composition of the histidine-based purification tag [13] and the design of the N- and C-terminus [14,15] on biodistribution were evaluated. It has also been found that the ADAPT6 provides the best imaging properties when a label is positioned at the C-terminus [16]. Furthermore, increased affinity of an ADAPT6 dimer does not counterbalance the disadvantage of increased size, since the monomeric form of ADAPT6 provides higher tumor uptake and better imaging contrast [17]. Based on these studies, an optimized variant of the imaging probe, $(HE)_3$DANS-ADAPT6-GSSC-DOTA, has been developed. The optimization reduced off-target interactions, which resulted in a several-fold increased tumor-to-liver and tumor-to-bone ratios. Since liver and bones are major metastatic sites, the optimized variant should improve HER2 detection in distant metastases.

The optimization was performed for labelling using the radionuclides ^{111}In ($T_{1/2}$ = 2.8 d) and ^{68}Ga ($T_{1/2}$ = 68 min). ^{111}In decays by electron capture accompanied by emission of gamma-quanta with energies of 171 keV (90%) and 245 keV (94%). This nuclide can be utilized for imaging based on single photon emission computed tomography (SPECT). For economic reasons, SPECT/CT cameras are the most commonly used imaging devices. The long half-life of ^{111}In permits its delivery world-wide. ^{68}Ga is a positron emitter (90% of decays), which enables the use of positron emission tomography (PET). PET imaging provides better spatial resolution, imaging sensitivity and quantification accuracy than SPECT, but its use is appreciably more expensive. However, ^{68}Ga is produced using a long-lived ^{68}Ge/^{68}Ga generator, which is much cheaper than cyclotron production of other positron emitters. Thus, selection of these nuclides for labelling should provide a facile clinical translation of a radiolabeled ADAPT6.

In previous studies, a maleimido derivative of macrocyclic chelator DOTA (1,4,7,10-tetraazacyclododecane-1,4,7,10-tetraacetic acid) was used for site-specific labelling of ADAPT6 with ^{111}In and ^{68}Ga. DOTA is a very versatile chelator providing thermodynamically stable and kinetically inert complexes with a large variety of metals, which permits its broad use in the radiopharmaceutical chemistry [18]. It has to be noted that stability of radionuclide attachment is only one, although a very important, aspect of selection of an optimal labelling strategy. Coupling of a metal-chelator complex to a polypeptide modifies its surface by changing the distribution of charges and thereby influence the lipophilicity of the water-exposed areas. It has been shown that position of a label and the chemical nature of the chelator as well as the radionuclide can modify binding affinity, internalization rate, and biodistribution properties of both short peptides and scaffold proteins [19]. Such impact of a chelator/radiometal combination is easily conceivable for short peptides, containing eight to ten amino acids. However, this influence is quite pronounced also for affibody molecules, which are similar in size with ADAPT6. The use of different chelators for labelling of affibody molecules with ^{111}In, ^{68}Ga, ^{89}Zr and ^{99m}Tc resulted in noticeable changes in uptake in normal tissues [20–23]. Furthermore, labelling of the same affibody-chelator conjugate with different nuclides also resulted in different biodistribution properties [22,24,25]. Similarly, DOTA-conjugated ADAPT6 had different blood clearance rates and biodistribution profiles when labelled with ^{111}In or ^{68}Ga [12,15]. By gaining knowledge about the influence of the labelling approach, selection of a variant that provides the highest tumor-to-organ rations and, accordingly, the best imaging contrast will be possible.

The goal of this study was to evaluate the biodistribution properties of $(HE)_3$DANS-ADAPT6-GSSC site-specifically labelled with ^{111}In and ^{68}Ga using maleimido derivatives of the macrocyclic chelators NOTA, NODAGA, DOTA and DOTAGA (Fig. 1) to select the best variants for SPECT and PET imaging.

2. Materials and methods

2.1. Reagents and instrumentation

$(HE)_3$DANS-ADAPT6-GSSC-NOTA, $(HE)_3$DANS-ADAPT6-GSSC-NODAGA, $(HE)_3$DANS-ADAPT6-GSSC-DOTA and $(HE)_3$DANS-GSSC-DOTAGA were produced, purified, and characterized based on the method described earlier [15,26]. ^{111}In-indium chloride was purchased from Mallinckrodt Sweden AB in the form of 0.01 M hydrochloric acid (HCl). ^{68}Ga was produced from a ^{68}Ge/^{68}Ga generator (Eckert and Ziegler) as a solution in 0.1 M HCl. The eluent was collected in fractions of 200 μL, and the highest radioactivity concentration fraction was used for radiolabeling. Buffers were prepared based on common methods from chemicals purchased from Merck (Darmstadt, Germany). For preparation of 0.2 M ammonium acetate, pH 5.5 and 1.25 M sodium acetate, pH 3.6, a Milli-Q water (resistance higher than 18 MΩ × cm) was used. Buffers for conjugation and labeling were purified by removing metal ion contamination using a Chelex 100 resin (Bio-Rad Laboratories, Richmond, USA).

HER2-expressing SKOV-3 ovarian carcinoma and BT-474 breast carcinoma cell lines were obtained from American Type Tissue Culture Collection (ATCC) via LGC Promochem, Borås, Sweden. Trypsin-EDTA solution (0.25% trypsin, 0.02% EDTA in buffer, Biochrom AG, Berlin, Germany) was used to detach the cells from the adherent flask/plate. Ketalar (ketamine, 50 mg/mL, Pfizer, NY, USA), Rompun (xylazin, 20 mg/mL, Bayer, Leverkusen, Germany), Heparin (5000 IE/mL, Leo Pharma, Köpenhamn, Danmark) were obtained commercially.

An automated gamma-counter with 3-inch NaI(Tl) detector (1480 WIZARD, Wallac Oy, Turku, Finland) was used for radioactivity measurements. VDC-405 ionization chamber (Veenstra Instruments BV, The Netherlands) was used for radioactivity measurements for formulation of injection solution. Quantitative analysis distribution in radio-instant thin layer chromatography (radio-ITLC) was performed using Cyclone Storage Phosphor System (Perkin Elmer Sweden AB, Stockholm,

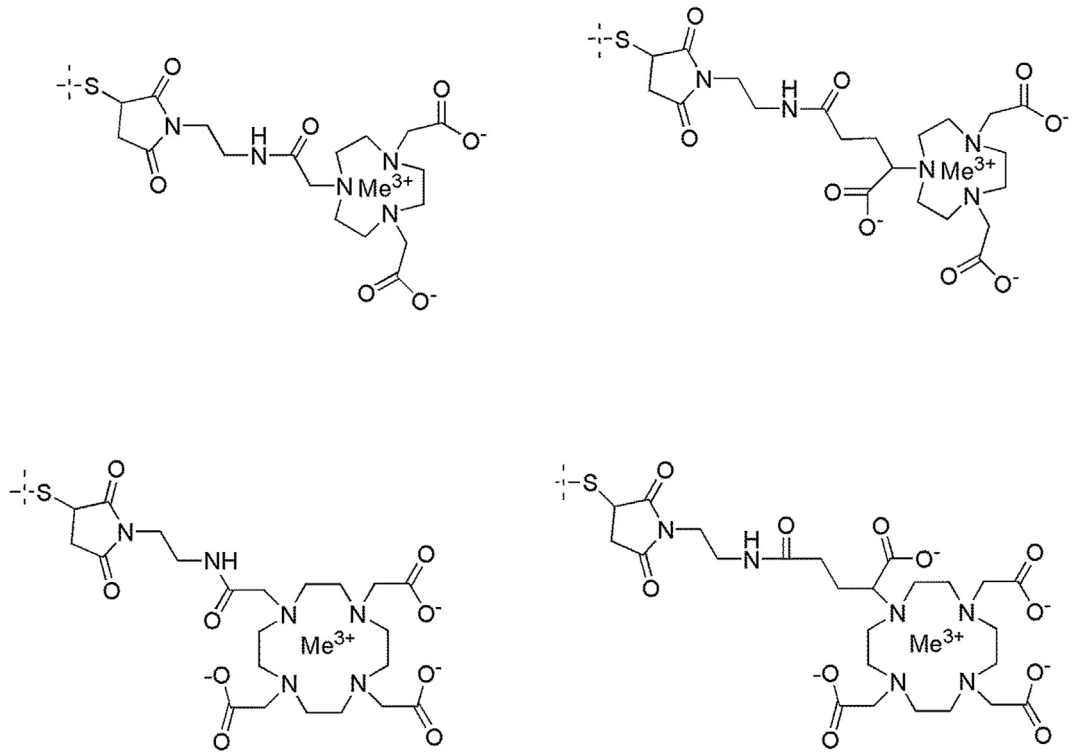

Fig. 1. Schematic drawing of NOTA, NODAGA, DOTA and DOTAGA maleimido derivatives conjugated to a cysteine.

Sweden). The identity of the conjugates labeled with ^{111}In was confirmed by reverse-phase high-performance liquid chromatography (RP-HPLC) on an Hitachi Chromaster HPLC system (Hitachi High-Tech Science Corporation, Tokyo, Japan) using an analytical column (Phenomenex LC Luna 5 µm C18(2) 100 Å, 150 × 4.6 mm, Ea) with a flow rate of 1 mL/min and a gradient of 5–70% B (A: 0.1% trifluoroacetic acid/H_2O, B: 0.1% trifluoroacetic acid/CH_3CN) over 15 min.

GraphPad Prism (version 4.00 for Windows GraphPad Software, San Diego California USA) was used for statistical analysis of difference in cellular binding and biodistribution data. A student unpaired, two tailed *t*-test was used to compare two groups. Difference between uptake of ^{68}Ga and ^{111}In in co-injection studies was investigated using paired *t*-test. For comparison of more than two sets of data in biodistribution studies, a one-way ANOVA with Bonferroni correction for multiple comparisons was used.

2.2. Labeling chemistry and in vitro studies

2.2.1. Labeling of chelator-conjugated ADAPT6 with ^{111}In

For labeling of ADAPT6-GSSC-NOTA, $(HE)_3$DANS-ADAPT6-GSSC-NODAGA, $(HE)_3$DANS-ADAPT6-GSSC-DOTA and $(HE)_3$DANS-ADAPT6-GSSC-DOTAGA with ^{111}In, 25 µg (4 nmol) of lyophilized chelator-conjugated ADAPT6 variants were reconstituted in 0.2 M ammonium acetate (pH 5.5) and incubated with 50 µL of ^{111}In solution (40–45 MBq in 0.05 M hydrochloric acid) at 95 °C for 40 min followed by challenging with 500-fold molar excess EDTA at 95 °C for 20 min. Before animal studies, traces of unbound ^{111}In were removed from radiolabeled ADAPT6 variants using disposable NAP-5 size-exclusion columns (GE Healthcare, Uppsala, Sweden). Radiochemical yield and purity of conjugates were determined using radio-ITLC. Identity of conjugates was confirmed using HPLC.

Stability of the radiolabeled conjugates was evaluated using radio-ITLC after incubating with a 500-fold molar excess of EDTA at room temperature for 2 h. The experiments were performed in duplicates, for control experiment the conjugates were incubated with PBS.

2.2.2. Labeling of chelator-conjugated ADAPT6 with ^{68}Ga

For labeling of $(HE)_3$DANS-ADAPT6-GSSC-NOTA, $(HE)_3$DANS-ADAPT6-GSSC-NODAGA, $(HE)_3$DANS-ADAPT6-GSSC-DOTA and $(HE)_3$DANS-ADAPT6-GSSC-DOTAGA with ^{68}Ga, 20 µg (3.2 nmol) of chelator-conjugated ADAPT6 was reconstituted in 40 µL 1.25 M sodium acetate buffer, pH 3.6. 100 µL of eluate containing ~70 MBq ^{68}Ga was added to the solution. The mixture was incubated at 95 °C for 15 min. Thereafter, tetrasodium salt of ethylene diamine tetraacetic acid (Na_4EDTA) (30 µL, 10 mg/mL) was added, and the mixture was further incubated at 95 °C for 5 min. Labeled conjugates were purified using NAP-5 size-exclusion columns. 1.5 µL was taken for analysis by radio-ITLC, eluted with 0.2 M citric acid. The ITLC was validated by HPLC.

Stability of the radiolabeled conjugates was evaluated using radio-ITLC after incubating with a 500-fold molar excess of EDTA at room temperature for 2 h. The experiments were performed in duplicates, for control experiment the conjugates were incubated with PBS.

2.3. In vitro binding specificity and cellular processing of bound conjugates by HER2-expressing cells

2.3.1. Testing specificity of binding to HER2-expressing cells

For *in vitro* studies, SKOV-3 and BT-474 cell lines were used. Approximately 1×10^6 cells per culture dish were seeded 1 day before experiment. For each chelator-conjugate, a set of six cell dishes was used. The binding specificity was tested by a saturation test. To saturate the receptors, 2.5 mM of unlabeled conjugate was added to 3 of these cell dishes 10 min before adding the labeled conjugate. The labeled conjugates with the concentration of 25 nM were added, and the cells were incubated for 1 h at 37 °C. Thereafter, the medium was aspirated, and cells were collected after washing twice with serum free media and detaching by trypsin. Radioactivity was measured in both the pre-saturated and unsaturated cells and percentage of cell-bound radioactivity was calculated.

2.3.2. Affinity determination using LigandTracer

SKOV-3 human ovarian carcinoma cells were seeded on a local area

of a cell culture dish (NunclonTM, Size 100620, NUNC A/S, Roskilde, Denmark), as described previously [27]. Affinity of binding of ^{111}In-labeled conjugates to HER2-expressing SKOV-3 human ovarian carcinoma cells was measured using LigandTracer Yellow instrument (Ridgeview Instruments AB). The recorded data were analyzed by Interaction Map software (Ridgeview Diagnostics AB) as described previously [27]. This device records kinetic binding and dissociation of radiolabeled tracers on living cells. For proper estimation, two increasing concentrations of each radioconjugate (1 and 3 nM) were used for affinity assay. Analysis was performed in duplicates. Interaction curves were analyzed to determine the affinity and rate constants using TraceDrawer evaluation software.

2.3.3. Cellular processing of conjugates bound to cancer cells in vitro

Processing of labeled conjugates by SKOV-3 and BT-474 cells during continuous incubation was investigated according to a method described earlier [26]. The labeled ADAPTs (protein concentration of 25 nM) were added to petri dishes containing 10^6 cells per culture dish. The cells were incubated at 37 °C, 5% CO_2 in a humidified atmosphere. At predetermined time points (1, 2, 4, 8 and 24 h for ^{111}In and, 1, 2 and 3 h for ^{68}Ga after addition), the media from 3 dishes was removed and the cells were washed twice with ice-cold serum-free medium. After treating the cells with 0.5 mL 0.2 M glycine buffer containing 4 M urea, pH 2.5, for 5 min on ice, the solution was collected. The cells were washed with an additional 0.5 mL glycine buffer and the fractions were pooled together (acid wash fractions). This fraction was considered as membrane-bound radioactivity. The cells were then incubated at 37 °C for at least 40 min with 0.5 mL 1 M NaOH. The alkaline solution was collected, the cell dishes were washed additionally with 0.5 mL NaOH and the alkaline fractions were pooled (base wash). This fraction was considered as internalized radioactivity. The radioactivity was measured and percentage of internalized radioactivity was calculated for each time point.

2.4. In vivo studies

Animal experiments were performed in agreement with national legislation on laboratory animal protection and were approved by the Ethics Committee for Animal Research in Uppsala (Permit Number: C4/2016). Efforts were made to minimize suffering of animals. Euthanasia was performed under ketamine/xylazine anesthesia.

Targeting properties and specificity of labeled ADAPTs were investigated in female BALB/C nu/nu mice bearing SKOV-3 xenografts. HER2-positive xenografts were established by subcutaneous implantation of 10^7 SKOV-3 in hind legs. For HER2-negative controls, $5x10^6$ Ramos cells were subcutaneously implanted. The average animal weight was 18 ± 1 g at the time of experiments. The average weight of xenografts was 0.38 ± 0.16 g and 0.35 ± 0.27 g for SKOV-3 and Ramos, respectively.

Targeting properties of ^{111}In- and ^{68}Ga-labeled ADAPT6 conjugates were compared by injection of mixture of both labels in the same mice. The labeled conjugates were formulated for co-injection based on the total injected protein mass of 10 μg per mouse. Biodistribution in mice bearing SKOV-3 xenografts was measured at 3 and 24 h p.i. Biodistribution in mice bearing Ramos xenografts was measured at 3 h p.i. For animals sacrificed at 3 h after injection, 700 kBq ^{68}Ga-labeled ADAPT6 and 10 kBq ^{111}In-labeled probe were mixed. For animals sacrificed at 24 h after injection, only 30 kBq of ^{111}In-labeled probe was used. Mice were sacrificed by i.p. injection of a lethal dose of anesthesia (ketamine, 10 mg/mL; xylazine, 1 mg/mL, 20 μL/g body weight) followed by heart puncture and exsanguination. Blood and organ samples were collected and weighed. Radioactivity of each nuclide in each sample was measured according to a previously described method [22]. These values were used to calculate uptake of ^{111}In- and ^{68}Ga-labeled ADAPT6 as percent of injected dose per gram tissue (%ID/g).

2.5. Imaging

Mice bearing SKOV-3 xenografts were injected with the best chelator-conjugate labeled with ^{68}Ga, ^{68}Ga-$(HE)_3$DANS-ADAPT6-GSSC-NODAGA (10 μg, 5 MBq) and ^{68}Ga- $(HE)_3$DANS-ADAPT6-GSSC-NOTA (10 μg, 4.5 MBq). Whole body PET scans were acquired using nanoScan PET/MRI (Mediso Medical Imaging Systems) at 3 h p.i. PET scans were performed for 30 min followed by CT examination at the same bed position using nanoScan SPECT/CT(Mediso Medical Imaging Systems). CT acquisition was performed using the following parameters: CT-energy peak of 50 keV, 670 μA, 480 projections, 5.2 min acquisition time. The PET data were reconstructed into a static image using the TeraTomo™ 3D reconstruction engine. The CT raw data were reconstructed using filtered back projection. PET and CT files were fused and analyzed using Nucline 2.03 Software (Mediso Medical Imaging Systems) and were presented as maximum intensity projections (MIP) in RGB color scale. For quantitative uptake evaluation, PET and CT data were fused and analyzed using PMOD v3.510 (PMOD Technologies Ltd., Zurich, Switzerland) and ROI were drawn manually at 50% of maximum uptake in tumors and kidneys.

3. Results

3.1. Protein production, purification, conjugation, and characterization

$(HE)_3$DANS-ADAPT6-GSSC was successfully produced in *E. coli*, harvested, and purified to homogeneity. The purified protein was efficiently conjugated with four different chelators, maleimide-NOTA/NODAGA/DOTA/DOTAGA, and their molecular weights were confirmed by mass spectrometry (Table 1). The final purity for all constructs was determined to be above 98% by reverse-phase high-performance liquid chromatography (Supplementary Fig S.1). Circular dichroism measurements showed high α-helical content (Supplementary Fig S.2), and high and equal melting temperatures for all conjugates (Table 1). All constructs also demonstrated excellent refolding ability after thermal denaturation (Supplementary Fig S.2). The affinities were determined using surface plasmon resonance to 1.0 nM, 3.3 nM, 4.5 nM and 2.2 nM for $(HE)_3$DANS-ADAPT6-GSSC-NOTA, $(HE)_3$DANS-ADAPT6-GSSC-NODAGA, $(HE)_3$DANS-ADAPT6-GSSC-DOTA and $(HE)_3$DANS-ADAPT6-GSSC-DOTAGA, respectively (Table 1). These values are comparable with the affinity value for the parental ADAPT6 molecule (2.5 nM) [12].

Table 1
Biophysical Characteristics of chelator-conjugated ADAPT6 Variants.

	Theoretical molecular weight (Da)	Measured molecular weight (Da)	T_m (°C)	K_D (nM) as determined by SPR measurements
$(HE)_3$DANS-ADAPT6-GSSC-NOTA	7101.88	7100.56	60	1.0
$(HE)_3$DANS-ADAPT6-GSSC- NODAGA	7173.94	7173.58	60	3.3
$(HE)_3$DANS-ADAPT6-GSSC-DOTA	7202.98	7202.61	60	4.5
$(HE)_3$DANS-ADAPT6-GSSC-DOTAGA	7275.04	7274.64	60	2.2

T_m, melting point; K_D, equilibrium dissociation constant; SPR, surface plasmon resonance.

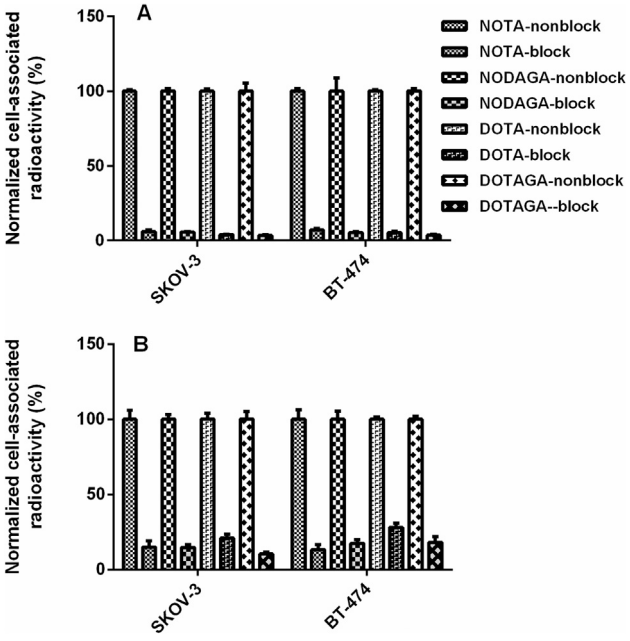

Fig. 2. *In vitro* specificity test of ^{111}In-labeled conjugates (A) and ^{68}Ga-labeled conjugates (B) to HER2 expressing SKOV-3 and BT-474 cells. Dishes containing cells were incubated with 25 nM radiolabeled ADAPT6. Data are normalized to maximum average cell-associated activity for each conjugate. Data are presented as mean values with standard deviations from three cell dishes.

3.2. Radiolabeling and label stability.

The radiochemical yields of labeling for ^{111}In- and ^{68}Ga-labeled NOTA, NODAGA, DOTA and DOTAGA conjugates of $(HE)_3$DANS-ADAPT6-GSSC were 92.5 ± 0.7%, 95 ± 1.4%, 82 ± 1.4% and 95 ± 2.8%, and, 79 ± 21%, 95 ± 4%, 36 ± 15% and 66 ± 29%, respectively. Size-exclusion chromatography purification provided a radiochemical purity of more than 99% and 96% for ^{111}In- and ^{68}Ga-labeled conjugates respectively. Apparent molar activity of ^{111}In-labeled conjugates was up to 11 GBq/μmol, and of ^{68}Ga-labeled conjugates up to 20 GBq/μmol. No release of radioactivity under challenge with 1000-fold excess of EDTA during 2 h was detected for any of the conjugates, as the differences between the control samples were within accuracy of the analytical method.

3.3. In vitro binding specificity and cellular processing of bound conjugates by HER2-expressing cells

The results of the specificity test for all ^{111}In- and ^{68}Ga-labeled conjugates binding to HER2-expressing cells are presented in Fig. 2. There was significantly lower binding ($p < 5 \times 10^{-5}$) of all eight conjugates to the HER2-expressing SKOV-3 and BT-474 cells (Fig. 2) treated with a large excess of non-labeled constructs. This demonstrated that the binding was saturable and indicated preserved binding specificity after radiolabeling of conjugates.

3.4. Affinity of binding to living HER2-expressing cells

The LigandTracer sensorgrams of the binding of all ^{111}In-labelled ADAPT6 variants to living cells (Supplementary Figs. S3 and S4) were best fitted to a 1:2 interaction model according to Langmuir. This indicates the presence of two types of interactions, one in the picomolar range and another in the low nanomolar range. Dissociation equilibrium constant (K_D) values for the interaction between ^{111}In-labelled ADAPT6 variants and HER2-expressing SKOV-3 cells are presented in Table 2.

Table 2
Dissociation equilibrium constants (KD) for the interaction of radiolabelled ADAPT6 variants with HER2-expressing SKOV-3 cells, determined using the TraceDrawer software.

	K_{D1}	K_{D2}
$(HE)_3$DANS-ADAPT6-GSSC-NOTA	35 ± 13 pM	4.1 ± 1.5 nM
$(HE)_3$DANS-ADAPT6-GSSC-NODAGA	17 ± 2 pM	3.7 ± 0.8 nM
$(HE)_3$DANS-ADAPT6-GSSC-DOTA	76 ± 14 pM	3.0 ± 0.1 nM
$(HE)_3$DANS-ADAPT6-GSSC-DOTAGA	28 ± 15 pM	3.4 ± 0.3 nM

Data concerning binding and processing of ^{111}In- and ^{68}Ga-labeled conjugates are presented in Figs. 3 and 4. The results show that the pattern was very similar for all conjugates and independent of cell line. The binding was rapid during the first hour of incubation with labeled conjugates, however, the increase of cell-bound radioactivity was slower thereafter. Internalization rate was quite slow for all variants. The internalization pattern of the conjugates tested in this study was in agreement with the data obtained earlier [26].

3.5. In vivo studies

Biodistribution of ^{111}In-conjugates and ^{68}Ga-conjugates in BALB/C nu/nu mice bearing SKOV-3 xenografts is shown in Fig. 5 and Table 3. The specificity of HER2 targeting *in vivo* was demonstrated by the use of HER2-negative Ramos xenografts (Fig. 5). The uptake of all ^{111}In-conjugates and ^{68}Ga-conjugates in SKOV-3 xenografts was significantly ($p < 0.0005$) higher in SKOV-3 than in Ramos xenografts, which indicated HER2-dependent accumulation.

All ^{68}Ga- and ^{111}In-conjugates demonstrated efficient clearance from blood and low uptake in normal organs and tissues except kidneys (Table 3). Uptake of radioactivity in tumor exceeded by far the uptakes in any normal tissues except kidneys. High uptake in kidneys is typical for small scaffold proteins, indicating glomerular filtration with subsequent re-absorption. The chelators had no profound influence on tumor uptake. The tumor uptake value of ^{111}In-conjugates was slightly, but significantly ($p < 0.05$) higher for NOTA than for DOTAGA at 24 h after injection.

The conjugates demonstrated profoundly different uptake in normal tissues (Table 3) resulting in a noticeable difference in tumor-to-organ ratios (Table 4). The use of the tetraaza chelators DOTA and DOTAGA for labelling with ^{111}In provided faster clearance from blood and normal tissues at both studied time points. Consequently, these chelators provided the highest tumor-to-organ ratios, since the tumor uptakes were similar. Notably, the liver uptake for ^{111}In-labeled DOTA-conjugated ADAPT6 was significantly lower than for the DOTAGA-conjugated variant ($p < 0.05$). Accordingly, DOTA provided the highest tumor-to-liver ratio at 24 h after injection (72 ± 23 vs 39 ± 7 for ^{111}In $(HE)_3$DANS-ADAPT6-GSSC-NODAGA).

The difference between the ^{68}Ga-labeled conjugates was not as pronounced as in the case of ^{111}In. ^{68}Ga-$(HE)_3$DANS-ADAPT6-GSSC-NODAGA provided significantly higher tumor-to-blood and tumor-to-liver ratios compared to DOTA- and DOTAGA-conjugated counterparts.

3.6. Imaging

The results of the small animal PET/CT imaging are presented in Fig. 6. ^{68}Ga-$(HE)_3$DANS-ADAPT6-GSSC-NODAGA (10 μg, 5 MBq) and ^{68}Ga-$(HE)_3$DANS-ADAPT6-GSSC-NOTA (10 μg, 4.5 MBq) were capable of imaging SKOV-3 xenografts. Average tumor SUVs were 1.3 ± 0.1 and 1.1 ± 0.1, for ^{68}Ga-$(HE)_3$DANS-ADAPT6-GSSC-NODAGA and ^{68}Ga-$(HE)_3$DANS-ADAPT6-GSSC-NOTA, respectively. Average kidney SUVs were 18.8 ± 0.6 and 1.1 ± 0.1, for ^{68}Ga-$(HE)_3$DANS-ADAPT6-GSSC-NODAGA and ^{68}Ga-$(HE)_3$DANS-ADAPT6-GSSC-NOTA, respectively. No other organs or tissues were visualized, which prevented drawing ROIs and quantitative assessment.

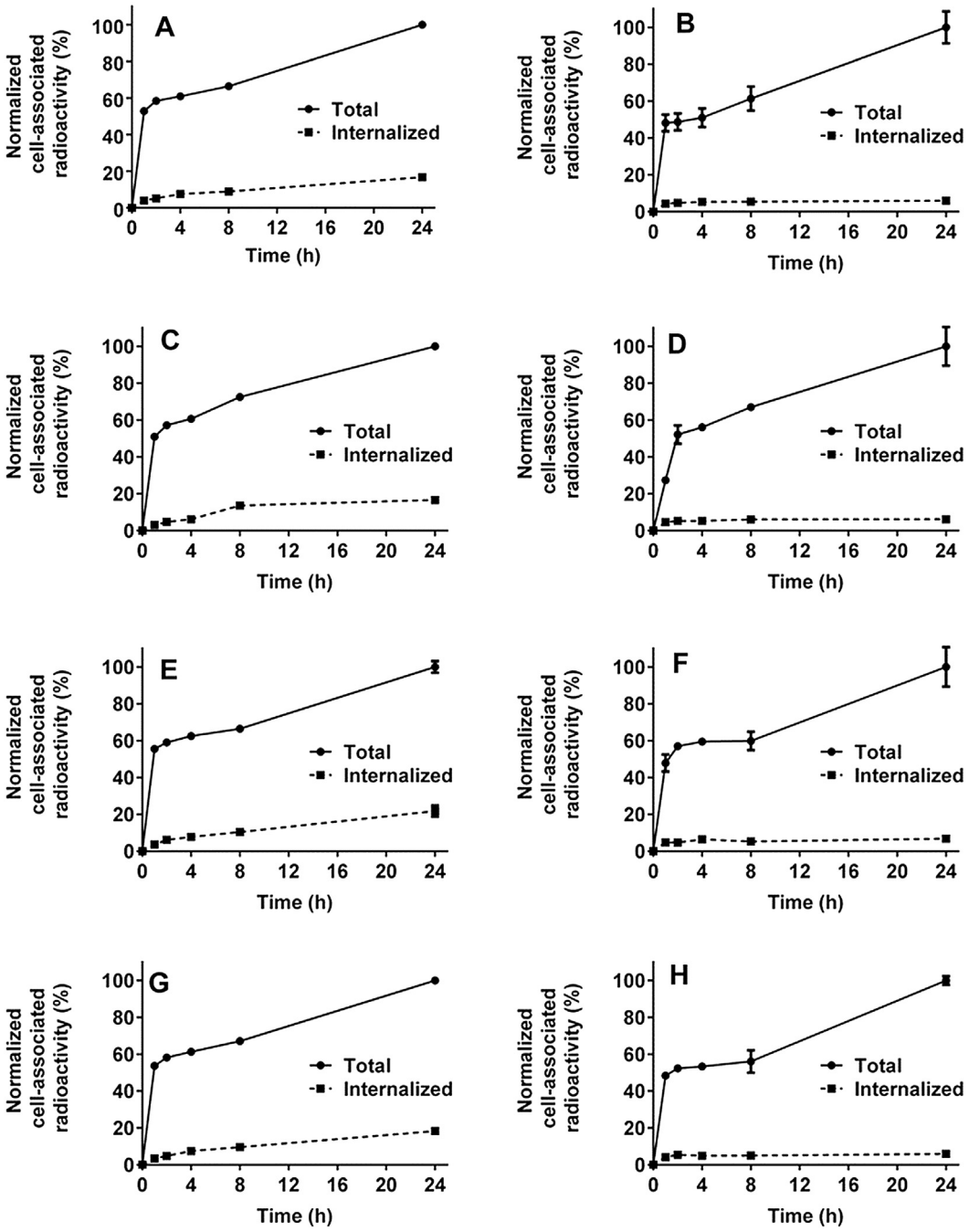

Fig. 3. Cellular processing of ^{111}In-(HE)$_3$DANS-ADAPT6-GSSC-NOTA (A, B), ^{111}In-(HE)$_3$DANS-ADAPT6-GSSC-NODAGA (C, D), ^{111}In-(HE)$_3$DANS-ADAPT6-GSSC-DOTA (E, F), ^{111}In-(HE)$_3$DANS-ADAPT6-GSSC-DOTAGA (G, H) by HER2-expressing SKOV-3 (A, C, E, G) and BT-474 (B, D, F, H) cell lines. Data are normalized to a maximum average cell-associated activity for each conjugate. Data are presented as mean values with standard deviations from three cell dishes.

4. Discussion

ESP are rather new types of imaging probes and so far, structure-properties relationships have been studied in details only for one class of ESP-based agents, affibody molecules. Importantly, these probes share only one common feature, a rigid scaffold. The primary, secondary and tertiary structures may differ substantially among the different ESP, and the chemical nature of the surface exposed amino acids in the various scaffolds are very different, which results in different biodistribution features. For example, the substitution of a hexahistidine tag by a histidine-glutamate (HE)$_3$-tag in affibody molecules resulted in a six-fold decrease in hepatic uptake [28]. The same substitution in DARPins resulted only in a three-fold decrease [29]. For ADAPT6, this effect was negligible [13]. Thus, information concerning structure-properties relationship for one ESP cannot be directly translated to the molecular design of another, but rather suggests which factors should be investigated. One such factor is the combination of a radionuclide and a chelator for its coupling to the ESP.

The goal of this study was to test the hypothesis that a combination of the commonly used macrocyclic chelators with the frequently used radionuclides, ^{111}In and ^{68}Ga, would result in radiolabelled (HE)$_3$DANS-ADAPT6-GSSC conjugates having different biodistribution profiles. Maleimido derivatives of the macrocyclic chelators NOTA, NODAGA, DOTA and DOTAGA were site-specifically conjugated to a unique cysteine at the C-terminus of the protein, and conjugates were purified to a high purity (above 98%, Supplementary Fig. S1). The

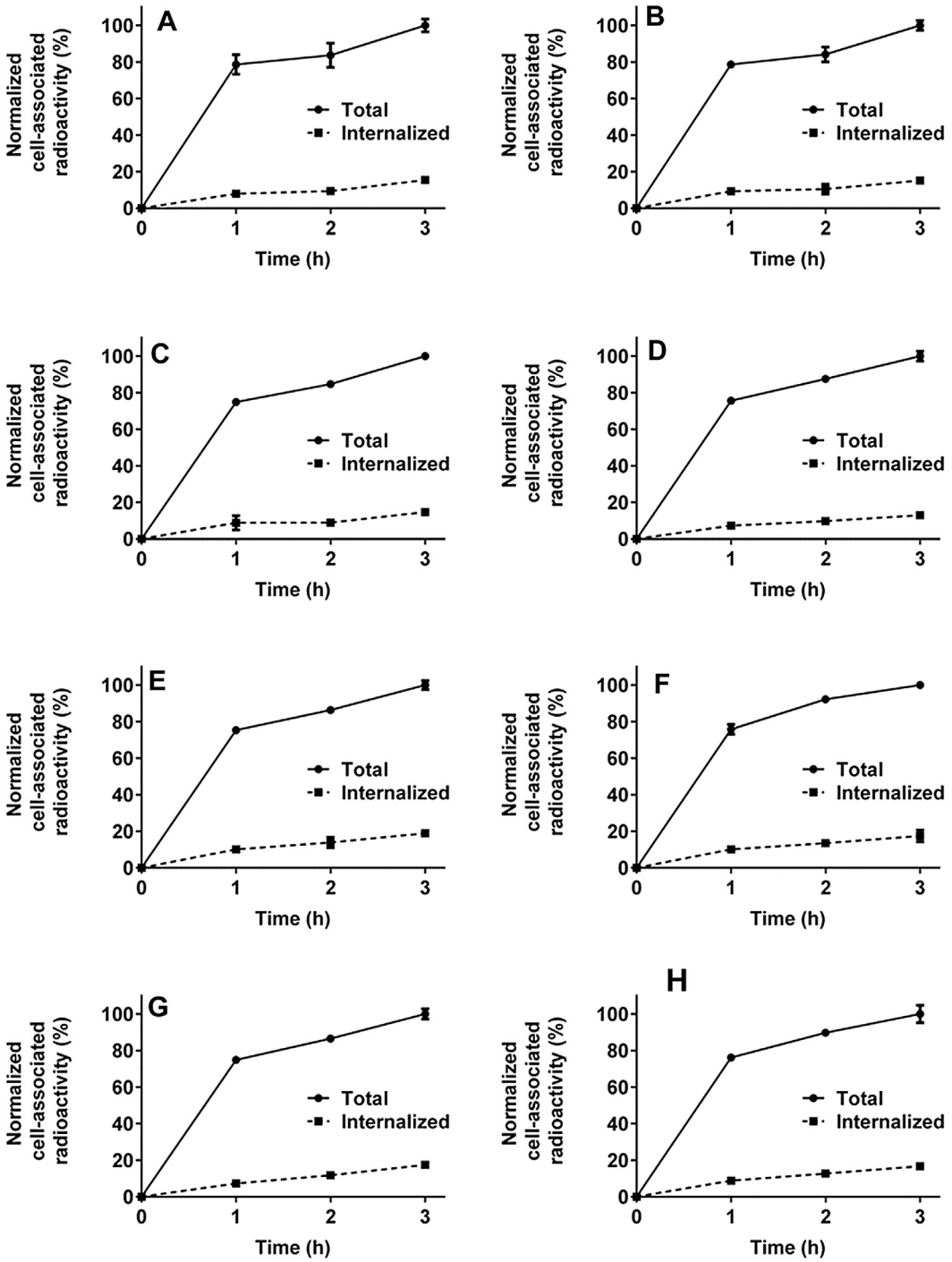

Fig. 4. Cellular processing of ^{68}Ga-(HE)$_3$DANS-ADAPT6-GSSC-NOTA (A, B), ^{68}Ga-(HE)$_3$DANS-ADAPT6-GSSC-NODAGA (C, D), ^{68}Ga-(HE)$_3$DANS-ADAPT6-GSSC-DOTA (E, F), ^{68}Ga-(HE)$_3$DANS-ADAPT6-GSSC-DOTAGA (G, H) by HER2-expressing SKOV-3 (A, C, E, G) and BT-474 (B, D, F, H) cell lines. Data are normalized to a maximum average cell-associated activity for each conjugate. Data are presented as mean values with standard deviations from three cell dishes.

radiolabeling was very efficient, and the use of size-exclusion chromatography provided high radiochemical purity. Due to kinetic inertness, radiolabeling using macrocyclic chelators often requires elevated temperatures. This might be associated with the risk of protein denaturation. However, an important feature of ADAPTs is their rapid refolding at physiologic temperature [8], a feature demonstrated to be true also for the specific conjugates of this study (Supplementary Fig S2). Indeed, all variants preserved specific binding to HER2-expressing cell lines *in vitro* after labelling (Fig. 2) and had similar affinity to HER2 (Table 2). The measurements of kinetics of binding to and dissociation from living cells using LigandTracer suggest that there are two different types of interactions between ADAPT6 variants and receptors. This phenomenon has been observed earlier for targeting proteins binding to dimerizing tyrosine kinase receptors [14,16,23], and might be associated with conformational changes caused by homodimerization of HER2 on the cells surface.

For short octapeptide somatostatin analogues, the internalization rate depends on the combination of the radionuclide and the chelator used for labelling [30–33]. The difference in internalization rate was essentially not pronounced for ADAPT6 variants (Figs. 3 and 4). This is

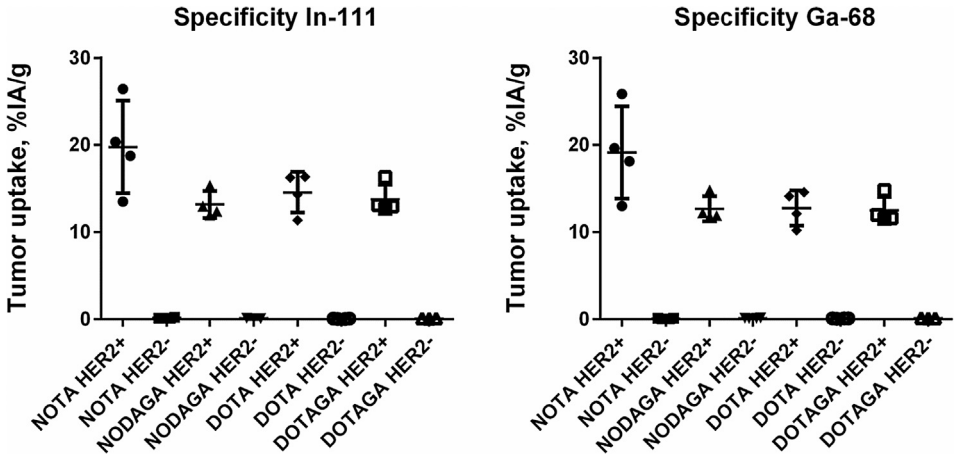

Fig. 5. *In vivo* HER2 targeting specificity of ^{111}In-conjugates (left), and ^{68}Ga-conjugates (right) in mice bearing SKOV-3 xenografts at 3 h p.i. Ramos xenografts were used as a HER2-negative control. Data, mean %ID/g ± SD (n = 4). The total injected radiolabeled protein dose per mouse was 10 μg.

Table 3
Comparative biodistribution values of ^{111}In/^{68}Ga-labeled ADAPT6 variants in BALB/C nu/nu mice bearing SKOV-3 xenografts (4 h pi). Data are presented as mean values with standard deviations from four mice.

	NOTA	NODAGA	DOTA	DOTAGA
3 h, ^{111}In-label				
blood	0.62 ± 0.10[b,c,g,h]	0.49 ± 0.05[d,e,g,h]	0.13 ± 0.02[b,d,f,g,h]	0.17 ± 0.01[c,e,f,g]
lung	0.46 ± 0.16[b,c,g]	0.41 ± 0.15[d,e,g,h]	0.16 ± 0.03[b,d,g,h]	0.17 ± 0.02[c,e,g,h]
liver	0.56 ± 0.13[b,c,h]	0.48 ± 0.09[d,e,g,h]	0.28 ± 0.03[b,d,f,g,h]	0.35 ± 0.03[c,e,f,g,h]
spleen	0.36 ± 0.12[b,c]	0.21 ± 0.06	0.20 ± 0.02[b,g,h]	0.18 ± 0.05[c]
stomach	0.17 ± 0.04[b,g]	0.10 ± 0.10	0.07 ± 0.02[b,h]	0.11 ± 0.04[g]
kidney	351 ± 60[g,h]	372 ± 46[g]	350 ± 21[f,g,h]	387 ± 14[f,g]
tumor	20 ± 5[g,h]	13 ± 2	15 ± 2[h]	14 ± 2[g,h]
muscle	0.08 ± 0.02[c,h]	0.11 ± 0.06[e]	0.04 ± 0.02[h]	0.04 ± 0.01[c,e]
bone	0.27 ± 0.08[b,g]	0.38 ± 0.17[d]	0.09 ± 0.04[b,d,f]	0.21 ± 0.08[d,f]
GI	0.59 ± 0.09[g,h]	0.43 ± 0.14[h]	0.43 ± 0.17[g]	0.45 ± 0.25
Carcass	3.99 ± 2.13[h]	2.26 ± 0.40[e,g,h]	1.74 ± 0.87[g]	1.39 ± 0.18[e]
3 h, ^{68}Ga-label				
blood	0.25 ± 0.05[a,h]	0.12 ± 0.02[a,d,e,h]	0.20 ± 0.02[d,h]	0.19 ± 0.01[e]
lung	0.28 ± 0.04	0.20 ± 0.07[h]	0.24 ± 0.04[h]	0.24 ± 0.03[h]
liver	0.40 ± 0.08[b,h]	0.28 ± 0.06[d,e,h]	0.79 ± 0.08[b,d,f,h]	0.41 ± 0.02[e,f,h]
spleen	0.29 ± 0.06[b]	0.21 ± 0.05[d]	0.52 ± 0.04[h]	0.25 ± 0.04
stomach	0.18 ± 0.06	0.14 ± 0.03	0.15 ± 0.03[h]	0.15 ± 0.02
kidney	366 ± 63[h]	376 ± 45[f]	338 ± 22[f,h]	380 ± 10[f]
tumor	19 ± 5[h]	13 ± 1	13 ± 2[h]	12 ± 2[h]
muscle	0.06 ± 0.01[h]	0.07 ± 0.02	0.07 ± 0.02[h]	0.05 ± 0.01
bone	0.19 ± 0.08	0.16 ± 0.02[e]	0.19 ± 0.07	0.25 ± 0.05[e]
GI *	0.50 ± 0.07[a,b,h]	0.29 ± 0.12[a,h]	0.36 ± 0.05[b]	0.48 ± 0.26
Carcass*	3.13 ± 2.05[a,h]	1.17 ± 0.36[a,d,h]	2.10 ± 0.57[d]	1.40 ± 0.16
24 h, ^{111}In-label				
blood	0.16 ± 0.02[c,g]	0.11 ± 0.03[d,e,g]	0.03 ± 0.01[d,f,g]	0.05 ± 0.01[c,e,f,g]
lung	0.15 ± 0.02[c,g]	0.14 ± 0.02[d,e,g]	0.08 ± 0.02[d,g]	0.06 ± 0.01[c,e,g]
liver	0.40 ± 0.07[c]	0.32 ± 0.04[a,d,g]	0.14 ± 0.02[b,d,f,g]	0.30 ± 0.02[c,f,g]
spleen	0.22 ± 0.02[c]	0.20 ± 0.04[d]	0.10 ± 0.03[d,f,g]	0.14 ± 0.01[c,f]
stomach	0.07 ± 0.02[c,g]	0.12 ± 0.03	0.07 ± 0.05	0.04 ± 0.00[c,g]
kidney	249 ± 33[b,c,g]	281 ± 56g	283 ± 49[b,g]	300 ± 13[c,g]
tumor	9 ± 1[c,g]	10 ± 2	10 ± 4	11 ± 1[c,g]
muscle	0.05 ± 0.02[c]	0.06 ± 0.03	0.03 ± 0.01	0.03 ± 0.01[c]
bone	0.14 ± 0.04g	0.36 ± 0.11[a,d,e,g]	0.05 ± 0.01[d,f]	0.18 ± 0.07[e,f]
GI*	0.26 ± 0.02g	0.25 ± 0.08[d]	0.12 ± 0.03[d,g]	0.85 ± 1.42
Carcass*	2.79 ± 1.85	1.50 ± 0.14[d]	0.65 ± 0.07[d,g]	1.44 ± 0.75

* Data for gastrointestinal tract with content are presented as %ID/whole sample.
[a] Significant difference ($p < 0.05$) between NOTA-label and NODAGA-label.
[b] Significant difference ($p < 0.05$) between NOTA-label and DOTA-label.
[c] Significant difference ($p < 0.05$) between NOTA-label and DOTAGA-label.
[d] Significant difference ($p < 0.05$) between NODAGA-label and DOTA-label.
[e] Significant difference ($p < 0.05$) between NODAGA-label and DOTAGA-label.
[f] Significant difference ($p < 0.05$) between DOTA-label and DOTAGA-label.
[g] Significant difference ($p < 0.05$) between 3 h ^{111}In and 24 h ^{111}In.
[h] Significant difference ($p < 0.05$) between 3 h ^{111}In and 3 h ^{68}Ga 3.

Table 4
Tumor-to-organ ratio values of ^{111}In/^{68}Ga-labeled ADAPT6 variants in BALB/C nu/nu mice bearing SKOV-3 xenografts (4 h pi). Data are presented as mean values with standard deviations from four mice.

	NOTA	NODAGA	DOTA	DOTAGA
3 h, ^{111}In-label				
blood	32 ± 6[g,h]	27 ± 1[d,e,g,h]	109 ± 33[b,d,g,h]	85 ± 8[c,e,g,h]
lung	44 ± 5[g]	34 ± 8[d,e,g]	94 ± 34[b,d,h]	88 ± 4[c,e,g,h]
liver	35 ± 3[a,g,h]	28 ± 4[a,d,e,h]	50 ± 12[b,d,h]	39 ± 5[e,g]
spleen	58 ± 12[g]	68 ± 19	73 ± 20[g,h]	74 ± 10[g]
stomach	120 ± 22	245 ± 176	217 ± 23[b,h]	180 ± 104
kidney	0.06 ± 0.01[a,g,h]	0.04 ± 0.00[a]	0.04 ± 0.01	0.04 ± 0.00[c,g]
muscle	277 ± 119[h]	139 ± 53[d,e]	342 ± 100[d,h]	342 ± 23[e]
bone	81 ± 36	40 ± 18[h]	198 ± 135[h]	75 ± 42
3 h, ^{68}Ga-labeled				
blood	77 ± 15[h]	108 ± 21[d,e,h]	64 ± 13[d,h]	66 ± 7[e,h]
lung	70 ± 23	68 ± 21	55 ± 13[h]	52 ± 8[h]
liver	48 ± 6[b,e,h]	47 ± 8[d,e,h]	16 ± 3[b,d,f,h]	31 ± 5[d,e,f]
spleen	67 ± 18	63 ± 12[d]	24 ± 4[d,f,h]	49 ± 14[d,f]
stomach	113 ± 39	96 ± 22	92 ± 25[h]	87 ± 7
kidney	0.05 ± 0.01[a,c,h]	0.03 ± 0.00[a]	0.04 ± 0.00	0.03 ± 0.00[d]
muscle	333 ± 112[h]	202 ± 81	195 ± 51[h]	227 ± 40
bone	120 ± 68	85 ± 18[e,h]	73 ± 18[h]	57 ± 5[e]
24 h, ^{111}In-label				
blood	60 ± 7[b,c,g]	96 ± 28[d,e,g]	295 ± 87[b,d,g]	226 ± 18[c,e,g]
lung	61 ± 7[b,c,g]	73 ± 10[d,e,g]	134 ± 29[b,d]	182 ± 28[c,e,g]
liver	23 ± 4[a,b,c,g]	33 ± 6[a,d]	72 ± 23[b,d,f]	39 ± 7[c,f,g]
spleen	40 ± 4[b,c,g]	52 ± 13[d,e]	102 ± 11[b,d,f,g]	76 ± 8[c,e,f,g]
stomach	123 ± 47[c]	89 ± 11[e]	159 ± 82	267 ± 48[c,e]
kidney	0.04 ± 0.01[g]	0.04 ± 0.01	0.04 ± 0.01	0.04 ± 0.01[g]
muscle	163 ± 45[b,c]	197 ± 61[d,e]	382 ± 103[b,d]	540 ± 110[c,e]
bone	67 ± 19[a,b]	30 ± 9[a,d,e]	193 ± 70[b,d,f]	65 ± 33[e,f]

[a] Significant difference ($p < 0.05$) between NOTA-label and NODAGA-label.
[b] Significant difference ($p < 0.05$) between NOTA-label and DOTA-label.
[c] Significant difference ($p < 0.05$) between NOTA-label and DOTAGA-label.
[d] Significant difference ($p < 0.05$) between NODAGA-label and DOTA-label.
[e] Significant difference ($p < 0.05$) between NODAGA-label and DOTAGA-label.
[f] Significant difference ($p < 0.05$) between DOTA-label and DOTAGA-label.
[g] Significant difference ($p < 0.05$) between 3 h ^{111}In and 24 h ^{111}In.
[h] Significant difference ($p < 0.05$) between 3 h ^{111}In and 3 h ^{68}Ga 3.

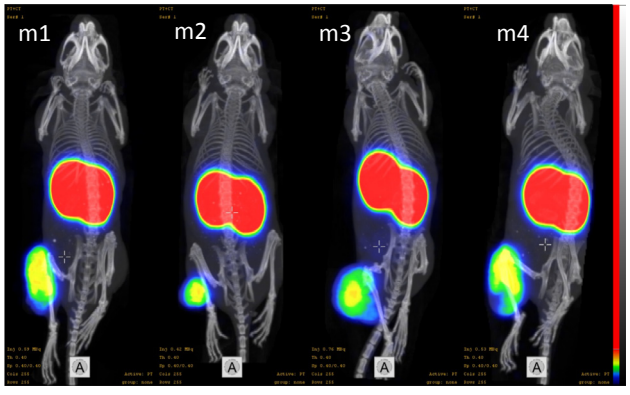

Fig. 6. Small animal PET/CT imaging of mice bearing HER2-expressing tumor xenografts after injection of ^{68}Ga-(HE)$_3$DANS-ADAPT6-GSSC-NODAGA (10 μg, 5 MBq, m1, m2) and ^{68}Ga-(HE)$_3$DANS-ADAPT6-GSSC-NOTA (10 μg, 4.5 MBq, m3, m4). Images were acquired at 3 h p.i. The upper SUV threshold was set to 3.0.

understandable when the difference in size is taken into account. In short peptides, the radiometal complex is a rather large part of the entire molecule and thereby it would possibly have a greater effect on the behavior of the peptide. This might not be the case for ADAPTs, which constitutes the main part of the imaging probe.

In vivo, all conjugates accumulated in human tumor xenografts in a HER2-specific manner (Fig. 5). The tumor uptake values were in a narrow range for all conjugates (Table 3). (HE)$_3$DANS-ADAPT6-GSSC-NOTA tended to provide higher tumor uptake, but the difference was significant ($p < 0.05$) only with the uptake value for (HE)$_3$DANS-ADAPT6-GSSC-DOTAGA. Tumor accumulation depends mainly on the hydrodynamic radii and the affinity of polypeptides [34]. Since these parameters are similar for all studied conjugates, the consistency in the tumor uptake values are not surprising.

There was however a profound difference between uptakes in normal tissues (Table 3) resulting in a striking difference in tumor-to-organ ratios (Table 4). For ^{111}In, the use of the tetraaza chelators DOTA and DOTAGA was associated with the most rapid clearance from blood and normal tissues at both studied time points. Accordingly, these chelators provided the highest tumor-to-organ ratios, since the tumor uptakes were similar. The tumor-to-organ ratios were similar for ^{111}In-(HE)$_3$DANS-ADAPT6-GSSC-DOTA and ^{111}In-(HE)$_3$DANS-ADAPT6-GSSC-DOTAGA, but the DOTA-containing variant provided significantly ($p < 0.05$) higher tumor-to-liver ratio at 24 h after injection (72 ± 23 vs 39 ± 7, respectively). Such a difference would enable better imaging of HER2-expression in small hepatic metastases frequently encountered in patients with breast and gastric cancers. Better imaging of such metastases is important, and ^{111}In-(HE)$_3$DANS-ADAPT6-GSSC-DOTA would be the preferable conjugate for SPECT imaging. In the case of ^{68}Ga label, the difference was not as pronounced as in the case of ^{111}In. Still, ^{68}Ga-(HE)$_3$DANS-ADAPT6-GSSC-DOTA was not the best variant, having higher uptake in liver and spleen compared to other counterparts. The best performing conjugate among the gallium-labelled constructs was ^{68}Ga-(HE)$_3$DANS-ADAPT6-GSSC-NODAGA, providing significantly higher tumor-to-blood and tumor-to-liver ratios compared to DOTA- and DOTAGA-conjugated counterparts.

High imaging contrast is an important precondition for sufficient sensitivity of radionuclide diagnostics. Particularly, it is important for imaging of small metastases. When the size of an imaged object is similar or less than the spatial resolution of the camera, the image will be blurred due to the so called partial volume effect (PVE) [35]. Therefore, the tumor-to-background ratio must be extremely high for imaging of small tumors [36]. While tumor uptake of the targeting protein is determined by size and affinity, the uptake in normal tissues is dependent on off-target interactions, including transient binding to blood proteins. The difference in charge between different radiometal-chelator complexes influences such off-target interactions, and results in different uptake in normal tissues. Moreover, the geometry of complexes of different nuclides with the same chelator might be different, which also influences the binding to blood and normal tissues. This might have a dramatic effect on short peptides, such as RGD derivatives or somatostatin and bombesin analogues [33,37,38]. However, influences of radiometal-chelator complexes has also been observed in larger ESP, including anti-HER and anti-EGFR affibody molecules [21,25]. This study exemplifies that the chelator-radiometal combination is apparently essential for ADAPTs as well.

Earlier, it has been demonstrated that the off-target interactions of monoclonal antibodies *in vitro* might be used for screening to identify antibodies with unusually fast clearance from blood [39]. To evaluate if this also was possible here, we analyzed the correlations between unspecific binding of the radiolabeled ADAPT6 variants *in vitro* and its uptake in normal tissues *in vivo* (Supplementary Fig. S5–S8). There was a surprisingly high correlation between unspecific binding of the different ^{111}In-labeled variants to SKOV-3 cells and its uptake in normal tissues (Supplementary Fig. S5). However, the correlation for BT-747 cell was somewhat lower. Furthermore, there was a very poor correlation for ^{68}Ga-labeled conjugates for all organs except liver and spleen. Overall, a correlation between unspecific binding *in vitro* and tissue uptake was reasonable only for liver and spleen (Fig. 7). Thus, due to the multitude of different interactions *in vivo* the influence of off-target interactions is very difficult to predict a priori which makes structure-

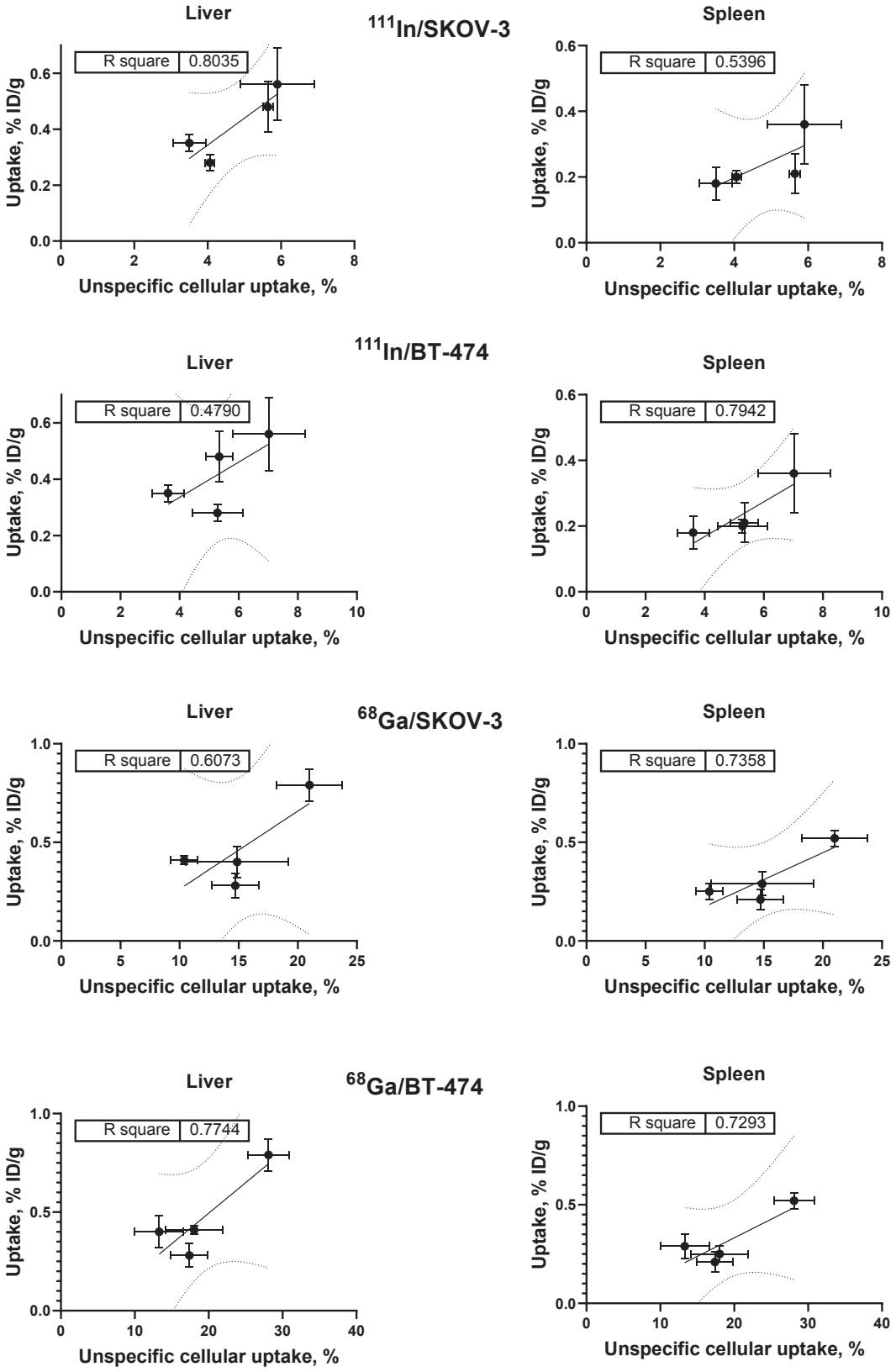

Fig. 7. Correlation between unspecific uptake of ^{111}In- and ^{68}Ga-labeled ADAPT6 variants *in vitro* and uptake in liver and spleen at 3 h after injection.

property relationship studies *in vivo*, as the presented one, necessary to select the best tracers for each clinical imaging modality.

5. Conclusions

Combination of a radionuclide and a chelator for its conjugation has a strong influence on uptake of ADAPT6 in normal tissues. This results in appreciable variation in tumor-to-organ ratios. The best variant for SPECT imaging is ^{111}In-(HE)$_3$DANS-ADAPT6-GSSC-DOTA while the best variant for PET imaging is ^{68}Ga-(HE)$_3$DANS-ADAPT6-GSSC-NODAGA. Studies concerning influence of labelling strategy on biodistribution are necessary to select a nuclide/chelator combination providing maximum sensitivity in imaging of molecular therapeutic target using radiolabeled engineered scaffold proteins.

Declaration of Competing Interest

The authors have no competing interests to declare.

Acknowledgements

This research was financially supported by grants from the Swedish Cancer Society [grants CAN 2018/436 and 2017/425], Swedish Research Council [grants 2015-02353 and 2015-02509], the Swedish Agency for Innovation VINNOVA (grant 2016-04060).

Appendix A. Supplementary material

Supplementary data to this article can be found online at https://doi.org/10.1016/j.ejpb.2019.05.008.

References

[1] M.J. Piccart-Gebhart, M. Procter, B. Leyland-Jones, A. Goldhirsch, M. Untch, I. Smith, L. Gianni, J. Baselga, R. Bell, C. Jackisch, D. Cameron, M. Dowsett, C.H. Barrios, G. Steger, C.-S. Huang, M. Andersson, M. Inbar, M. Lichinitser, I. Láng, U. Nitz, H. Iwata, C. Thomssen, C. Lohrisch, T.M. Suter, J. Rüschoff, T. Sütő, V. Greatorex, C. Ward, C. Straehle, E. McFadden, M.S. Dolci, R.D. Gelber, Trastuzumab after adjuvant chemotherapy in HER2-positive breast cancer, N. Engl. J. Med. 353 (2005) 1659–1672, https://doi.org/10.1056/NEJMoa052306.

[2] V. Diéras, D. Miles, S. Verma, M. Pegram, M. Welslau, J. Baselga, I.E. Krop, K. Blackwell, S. Hoersch, J. Xu, M. Green, L. Gianni, Trastuzumab emtansine versus capecitabine plus lapatinib in patients with previously treated HER2-positive advanced breast cancer (EMILIA): a descriptive analysis of final overall survival results from a randomised, open-label, phase 3 trial, Lancet Oncol. 18 (2017) 732–742, https://doi.org/10.1016/S1470-2045(17)30312-1.

[3] H. Joensuu, P.-L. Kellokumpu-Lehtinen, P. Bono, T. Alanko, V. Kataja, R. Asola, T. Utriainen, R. Kokko, A. Hemminki, M. Tarkkanen, T. Turpeenniemi-Hujanen, S. Jyrkkiö, M. Flander, L. Helle, S. Ingalsuo, K. Johansson, A.-S. Jääskeläinen, M. Pajunen, M. Rauhala, J. Kaleva-Kerola, T. Salminen, M. Leinonen, I. Elomaa, J. IsolaFinHer Study Investigators, Adjuvant docetaxel or vinorelbine with or without Trastuzumab for breast cancer, N. Engl. J. Med. 354 (2006) 809–820, https://doi.org/10.1056/NEJMoa053028.

[4] D.A. Mankoff, M.D. Farwell, A.S. Clark, D.A. Pryma, Making molecular imaging a clinical tool for precision oncology, JAMA Oncol. 3 (2017) 695, https://doi.org/10.1001/jamaoncol.2016.5084.

[5] V. Tolmachev, Imaging of HER-2 overexpression in tumors for guiding therapy, Curr. Pharm. Des. 14 (2008) 2999–3019.

[6] K.E. Henry, G.A. Ulaner, J.S. Lewis, Clinical potential of human epidermal growth factor receptor 2 and human epidermal growth factor receptor 3 imaging in breast cancer, PET Clin. 13 (2018) 423–435, https://doi.org/10.1016/j.cpet.2018.02.010.

[7] A. Krasniqi, M. D'Huyvetter, N. Devoogdt, F.Y. Frejd, J. Sörensen, A. Orlova, M. Keyaerts, V. Tolmachev, Same-day imaging using small proteins: clinical experience and translational prospects in oncology, J. Nucl. Med. 59 (2018) 885–891, https://doi.org/10.2967/jnumed.117.199901.

[8] J. Nilvebrant, S. Hober, The albumin-binding domain as a scaffold for protein engineering, Comput. Struct. Biotechnol. J. 6 (2013), https://doi.org/10.5936/csbj.201303009.

[9] J. Nilvebrant, M. Åstrand, J. Löfblom, S. Hober, Development and characterization of small bispecific albumin-binding domains with high affinity for ErbB3, Cell. Mol. Life Sci. 70 (2013) 3973–3985, https://doi.org/10.1007/s00018-013-1370-9.

[10] J. Nilvebrant, T. Alm, S. Hober, J. Lö fblom, Engineering bispecificity into a single albumin-binding domain, PLoS One. 6 (2011), https://doi.org/10.1371/journal.pone.0025791.

[11] J. Nilvebrant, M. Åstrand, M. Georgieva-Kotseva, M. Björnmalm, J. Löfblom, S. Hober, Engineering of bispecific affinity proteins with high affinity for ERBB2 and adaptable binding to albumin, PLoS One 9 (2014) e103094, https://doi.org/10.1371/journal.pone.0103094.

[12] J. Garousi, S. Lindbo, J. Nilvebrant, M. Astrand, J. Buijs, M. Sandstrom, H. Honarvar, A. Orlova, V. Tolmachev, S. Hober, ADAPT, a novel scaffold protein-based probe for radionuclide imaging of molecular targets that are expressed in disseminated cancers, Cancer Res. 75 (2015) 4364–4371, https://doi.org/10.1158/0008-5472.CAN-14-3497.

[13] S. Lindbo, J. Garousi, M. Åstrand, H. Honarvar, A. Orlova, S. Hober, V. Tolmachev, Influence of histidine-containing tags on the biodistribution of ADAPT scaffold proteins, Bioconjug. Chem. 27 (2016) 716–726, https://doi.org/10.1021/acs.bioconjchem.5b00677.

[14] J. Garousi, S. Lindbo, H. Honarvar, J. Velletta, B. Mitran, M. Altai, A. Orlova, V. Tolmachev, S. Hober, Influence of the N-terminal composition on targeting properties of radiometal-labeled anti-HER2 scaffold protein ADAPT6, Bioconjug. Chem. 27 (2016) 2678–2688, https://doi.org/10.1021/acs.bioconjchem.6b00465.

[15] S. Lindbo, J. Garousi, B. Mitran, A. Vorobyeva, M. Oroujeni, A. Orlova, S. Hober, V. Tolmachev, Optimized molecular design of ADAPT-based HER2-imaging probes labeled with ^{111}In and ^{68}Ga, Mol. Pharm. 15 (2018) 2674–2683, https://doi.org/10.1021/acs.molpharmaceut.8b00204.

[16] S. Lindbo, J. Garousi, B. Mitran, M. Altai, J. Buijs, A. Orlova, S. Hober, V. Tolmachev, Radionuclide tumor targeting using ADAPT scaffold proteins: aspects of label positioning and residualizing properties of the label, J. Nucl. Med. 59 (2018) 93–99, https://doi.org/10.2967/jnumed.117.197202.

[17] J. Garousi, S. Lindbo, J. Borin, E. von Witting, A. Vorobyeva, M. Oroujeni, B. Mitran, A. Orlova, J. Buijs, V. Tolmachev, S. Hober, Comparative evaluation of dimeric and monomeric forms of ADAPT scaffold protein for targeting of HER2-expressing tumours, Eur. J. Pharm. Biopharm. 134 (2019) 37–48, https://doi.org/10.1016/j.ejpb.2018.11.004.

[18] E.W. Price, C. Orvig, Matching chelators to radiometals for radiopharmaceuticals, Chem. Soc. Rev. 43 (2014) 260–290, https://doi.org/10.1039/c3cs60304k.

[19] V. Tolmachev, A. Orlova, Influence of labelling methods on biodistribution and imaging properties of radiolabelled peptides for visualisation of molecular therapeutic targets, Curr. Med. Chem. 17 (2010) 2636–2655.

[20] H. Wallberg, A. Orlova, M. Altai, S.J. Hosseinimehr, C. Widstrom, J. Malmberg, S. Stahl, V. Tolmachev, Molecular design and optimization of 99mTc-labeled recombinant affibody molecules improves their biodistribution and imaging properties, J. Nucl. Med. 52 (2011) 461–469, https://doi.org/10.2967/jnumed.110.083592.

[21] J. Malmberg, A. Perols, Z. Varasteh, M. Altai, A. Braun, M. Sandström, U. Garske, V. Tolmachev, A. Orlova, A. Eriksson Karlström, Comparative evaluation of synthetic anti-HER2 Affibody molecules site-specifically labelled with 111In using N-terminal DOTA, NOTA and NODAGA chelators in mice bearing prostate cancer xenografts, Eur. J. Nucl. Med. Mol. Imaging 39 (2012) 481–492, https://doi.org/10.1007/s00259-011-1992-9.

[22] J. Strand, H. Honarvar, A. Perols, A. Orlova, R.K. Selvaraju, A.E. Karlström, V. Tolmachev, Influence of macrocyclic chelators on the targeting properties of 68Ga-labeled synthetic affibody molecules: comparison with 111In-labeled counterparts, PLoS One 8 (2013), https://doi.org/10.1371/journal.pone.0070028.

[23] D. Summer, J. Garousi, M. Oroujeni, B. Mitran, K.G. Andersson, A. Vorobyeva, J. Löfblom, A. Orlova, V. Tolmachev, C. Decristoforo, Cyclic versus noncyclic chelating scaffold for ^{89} Zr-labeled ZEGFR:2377 affibody bioconjugates targeting epidermal growth factor receptor overexpression, Mol. Pharm. 15 (2018) 175–185, https://doi.org/10.1021/acs.molpharmaceut.7b00787.

[24] J. Garousi, K.G. Andersson, J.H. Dam, B.B. Olsen, B. Mitran, A. Orlova, J. Buijs, S. Ståhl, J. Löfblom, H. Thisgaard, V. Tolmachev, The use of radiocobalt as a label improves imaging of EGFR using DOTA-conjugated affibody molecule, Sci. Rep. 7 (2017) 5961, https://doi.org/10.1038/s41598-017-05700-7.

[25] M. Oroujeni, J. Garousi, K. Andersson, J. Löfblom, B. Mitran, A. Orlova, V. Tolmachev, Preclinical evaluation of [68Ga]Ga-DFO-ZEGFR:2377: a promising affibody-based probe for noninvasive PET imaging of EGFR expression in tumors, Cells 7 (2018) 141, https://doi.org/10.3390/cells7090141.

[26] J. Garousi, S. Lindbo, B. Mitran, J. Buijs, A. Vorobyeva, A. Orlova, V. Tolmachev, S. Hober, Comparative evaluation of tumor targeting using the anti-HER2 ADAPT scaffold protein labeled at the C-terminus with indium-111 or technetium-99m, Sci. Rep. 7 (2017) 14780, https://doi.org/10.1038/s41598-017-15366-w.

[27] V. Tolmachev, A. Orlova, K. Andersson, Methods for radiolabelling of monoclonal antibodies, in: Methods Mol. Biol., 2014, pp. 309–330. https://doi.org/10.1007/978-1-62703-586-6_16.

[28] C. Hofström, A. Orlova, M. Altai, F. Wångsell, T. Gräslund, V. Tolmachev, Use of a HEHEHE purification tag instead of a hexahistidine tag improves biodistribution of affibody molecules site-specifically labeled with ^{99m}Tc, ^{111}In, and ^{125}I, J. Med. Chem. 54 (2011) 3817–3826, https://doi.org/10.1021/jm200065e.

[29] R. Goldstein, J. Sosabowski, M. Livanos, J. Leyton, K. Vigor, G. Bhavsar, G. Nagy-Davidescu, M. Rashid, E. Miranda, J. Yeung, B. Tolner, A. Plückthun, S. Mather, T. Meyer, K. Chester, Development of the designed ankyrin repeat protein (DARPin) G3 for HER2 molecular imaging, Eur. J. Nucl. Med. Mol. Imaging 42 (2015) 288–301, https://doi.org/10.1007/s00259-014-2940-2.

[30] M. de Jong, W.A. Breeman, W.H. Bakker, P.P. Kooij, B.F. Bernard, L.J. Hofland, T.J. Visser, A. Srinivasan, M.A. Schmidt, J.L. Erion, J.E. Bugaj, H.R. Mäcke, E.P. Krenning, Comparison of (111)In-labeled somatostatin analogues for tumor scintigraphy and radionuclide therapy, Cancer Res. 58 (1998) 437–441.

[31] L.J. Hofland, W.A. Breeman, E.P. Krenning, M. de Jong, M. Waaijers, P.M. van Koetsveld, H.R. Mäcke, S.W. Lamberts, Internalization of [DOTA degrees,125I-Tyr3]Octreotide by somatostatin receptor-positive cells in vitro and in vivo: implications for somatostatin receptor-targeted radio-guided surgery, Proc. Assoc. Am.

Phys. 111 (1999) 63–69.
[32] M. Ginj, H. Zhang, K.-P. Eisenwiener, D. Wild, S. Schulz, H. Rink, R. Cescato, J.C. Reubi, H.R. Maecke, New pansomatostatin ligands and their chelated versions: affinity profile, agonist activity, internalization, and tumor targeting, Clin. Cancer Res. 14 (2008) 2019–2027, https://doi.org/10.1158/1078-0432.CCR-07-1687.
[33] A. Heppeler, J.P. André, I. Buschmann, X. Wang, J.-C. Reubi, M. Hennig, T.A. Kaden, H.R. Maecke, Metal-ion-dependent biological properties of a chelator-derived somatostatin analogue for tumour targeting, Chem. – A Eur. J. 14 (2008) 3026–3034, https://doi.org/10.1002/chem.200701264.
[34] M.M. Schmidt, K. Dane Wittrup, A modeling analysis of the effects of molecular size and binding affinity on tumor targeting, Mol. Cancer Ther. 8 (2009) 2861–2871, https://doi.org/10.1158/1535-7163.MCT-09-0195.
[35] M. Soret, S.L. Bacharach, I. Buvat, Partial-volume effect in PET tumor imaging, J. Nucl. Med. 48 (2007) 932–945, https://doi.org/10.2967/jnumed.106.035774.
[36] W.C. Eckelman, M.R. Kilbourn, C.A. Mathis, Specific to nonspecific binding in radiopharmaceutical studies: it's not so simple as it seems!, Nucl. Med. Biol. 36 (2009) 235–237, https://doi.org/10.1016/j.nucmedbio.2008.12.002.
[37] C. Decristoforo, I. Hernandez Gonzalez, J. Carlsen, M. Rupprich, M. Huisman, I. Virgolini, H.-J. Wester, R. Haubner, 68Ga- and 111In-labelled DOTA-RGD peptides for imaging of αvβ3 integrin expression, Eur. J. Nucl. Med. Mol. Imaging. 35 (2008) 1507–1515, https://doi.org/10.1007/s00259-008-0757-6.
[38] Z. Varasteh, B. Mitran, U. Rosenström, I. Velikyan, M. Rosestedt, G. Lindeberg, J. Sörensen, M. Larhed, V. Tolmachev, A. Orlova, The effect of macrocyclic chelators on the targeting properties of the 68 Ga-labeled gastrin releasing peptide receptor antagonist PEG 2 -RM26, Nucl. Med. Biol. 42 (2015) 446–454, https://doi.org/10.1016/j.nucmedbio.2014.12.009.
[39] O. Hötzel, F.P. Theil, L.J. Bernstein, S. Prabhu, D. Deng, L. Quintana, J. Lutman, R. Sibia, P. Chan, D. Bumbaca, P. Fielder, P.J. Carter, R.F. Kelley, A strategy for risk mitigation of antibodies with fast clearance, MAbs 4 (2012) 753–760, https://doi.org/10.4161/mabs.22189.